Bioconjugate Chemistry

Article

pubs.acs.org/bc

Mammary-Derived Growth Inhibitor Targeting Peptide-Modified PEG−PLA Nanoparticles for Enhanced Targeted Glioblastoma Therapy

Xingye Feng,[†] Xiaoling Gao,[‡] Ting Kang,[†] Di Jiang,[†] Jianhui Yao,[†] Yixian Jing,[†] Qingxiang Song,[‡] Xinguo Jiang,[†] Jianying Liang,*[,†] and Jun Chen*[,†]

[†]Key Laboratory of Smart Drug Delivery, Ministry of Education, School of Pharmacy, Fudan University, 826 Zhangheng Road, Shanghai, 201203, PR China

[‡]Department of Pharmacology, Institute of Medical Sciences, Shanghai Jiaotong University School of Medicine, 280 South Chongqing Road, Shanghai, 200025, PR China

ABSTRACT: Targeting delivery of chemotherapeutics to neovasculature represents a promising means for tumor therapy since angiogenesis has been a featured hallmark of glioblastma. However, anti-angiogenic therapy would induce the occurrence of metastatic tumor and even neoplasm recurrence. Simultaneous targeting of tumor cells and neovasculature perfectly overcome such defects and has been proven to be an efficacious strategy for suppressing tumor growth. In the present study, a tumor homing peptide CooP selective binding to mammary-derived growth inhibitor that overexpressed in glioma cells and blood vessel endothelial cells was decorated on the surface of paclitaxel-loading PEG−PLA nanoparticles (NP-PTX) to obtain the dual targeting nanovector CooP-NP-PTX. In vitro antiproliferation study showed that HUVEC cells and U87MG cells were much more sensitive to CooP-NP-PTX than NP-PTX. In vivo imaging demonstrated that CooP-NP accumulated more selectively and penetrated deeper into the tumor site. In addition, the glioma-bearing mice treated with CooP-NP-PTX achieved the longest survival time compared to NP-PTX and Taxol. The findings observed above indicated that CooP peptide-functionalized anti-neoplastic agent-loaded nanoparticles might possess promising potential for glioblastoma therapy.

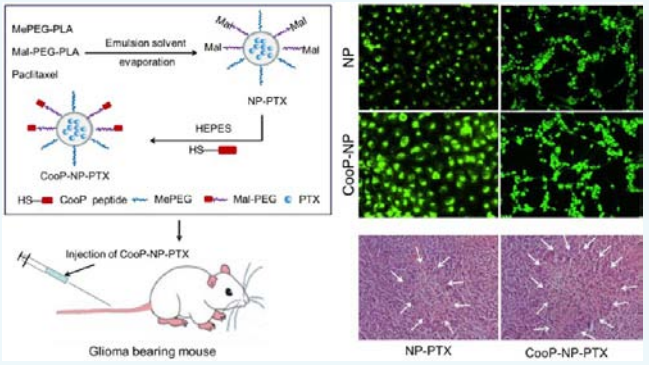

INTRODUCTION

Malignant astrocytic gliomas such as glioblastoma are the most common and lethal intracranial tumors, accounting for ∼40% of all primary brain tumors and 70% of all malignant gliomas. Glioblastoma is also one of the most vascularized and deadly cancers with a very low 5-year survival rate of 5%.[1−3] Although numerous strategies and improved methods have been developed for glioma therapy, the therapeutic effect was modest mainly due to the existing roadblocks such as the nonspecific, nontargeted nature of most of the drugs currently in use and the inadequate delivery of many drugs across the blood-brain barrier (BBB) and blood-tumor barrier (BTB).[4] Therefore, an effective glioma therapy is required for local, controlled, and precise delivery of chemotherapeutics.[5]

Controlling tumor-associated angiogenesis has been proven to be a promising tactic in limiting cancer progression, as angiogenesis plays a critical role in tumor growth and metastasis.[6] It has been reported that various strategies of anti-angiogenesis have a prominent effect of tumor inhibition.[7,8] Glioblastoma has been characterized with high degree of neo-angiogenesis,[9] and angiogenesis together with tumor cell invasion are essential for glioma development and growth, even in the earliest phases.[10] Anti-angiogenic therapy for glioma hence may be an efficient way because of several advantages when compared to conventional chemotherapy such as enhancing the "bystander effect",[11] directly exposing tumor vascular endothelial cells (EC) to the blood circulation, and evading the multidrug resistance of tumor cells.[12]

Although multiple strategies of inhibiting neo-angiogenesis have been confirmed to effectively suppress glioma to a larger extent in many preclinical studies, research recently has shown that antivascular therapy would increase the risk of local glioma invasion, evasive resistance, and distant metastasis through various mechanisms.[13−16] The main reason lies in increased vascular remodeling after anti-angiogenesis treatment leading to a more hypoxic tumor microenvironment, which consequently enhances tumor cell invasion.[17] Simultaneous targeting of neo-angiogenesis and tumor cells might represent an improved method since it not only severs the microcirculation paths which are indispensable for the tumor to obtain nutrients and

Received: July 7, 2015
Revised: July 27, 2015
Published: July 29, 2015

DOI: 10.1021/acs.bioconjchem.5b00379
Bioconjugate Chem. 2015, 26, 1850−1861

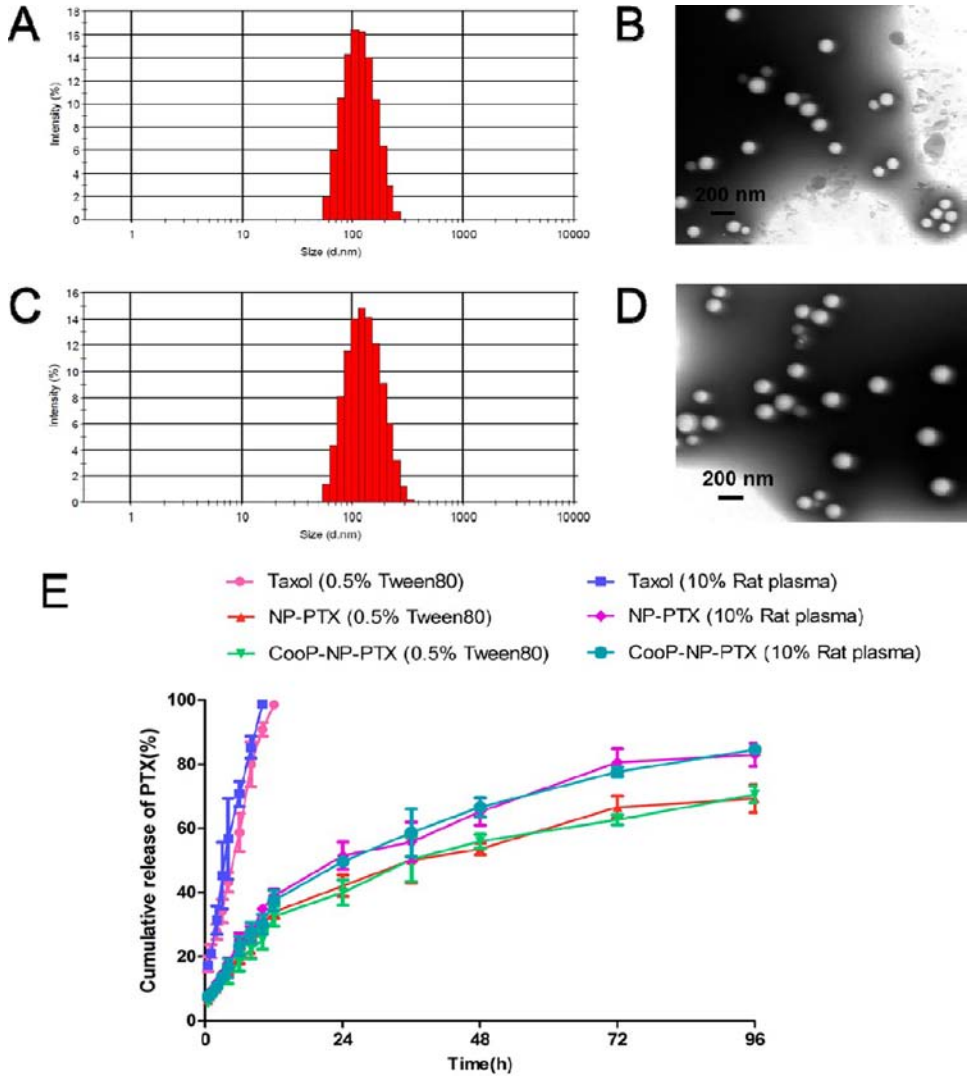

Figure 1. Characterization of NP and CooP-NP. Particle size distribution and TEM image of NP (A,B) and CooP-NP (C,D). PTX release profiles from Taxol, NP-PTX, and CooP-NP-PTX in PBS (pH 7.4) with 0.5% Tween-80 and PBS (pH 7.4) containing 10% rat plasma at 37 °C (E). The bar is 200 nm.

oxygen, but also penetrates into the tumor site to directly kill tumor cells.[18] Hence, dual-targeting therapy perfectly compensated for anti-angiogenic therapy only.

CooP was identified as a tumor-homing peptide, binding specifically to mammary-derived growth inhibitor (MDGI), also known as heart fatty acid-binding protein-(H-FABP/FABP3), through the technology of in vivo phage display.[19] MDGI is a member of the fatty acid-binding protein family of lipophilic intracellular proteins, which include retinoic acid binding proteins and related molecules.[20,21] In addition, MDGI has been considered to be the only FABP that affects cell proliferation and differentiation; however, this function is separate from its ligand binding function for its own mimicked C-terminal peptide to obstruct the binding with fatty acids.[22,23] Importantly, it has been reported that MDGI is overexpressed in some malignant tumors such as U87MG and BT4C tumors,[24] and its expression in glioma plays an important role in tumor progression and exhibits a grade-dependent manner.[25] As reported, MDGI is expressed in both glioma cells and blood vascular endothelium but not in normal brain,[19] which therefore provides an ideal target for delivering antitumor therapeutics to glioma through tumor cells and angiogenesis dual targeting.

In this study, PEG−PLA nanoparticles were prepared and functionalized with CooP peptide through a maleimide−thiol coupling reaction to deliver paclitaxel (PTX) to both glioma cells and vascular endotherial cells for enhanced antitumor efficacy. For in vitro assay, primary human umbilical vein endothelial cells (HUVEC) and U87 glioma cells were used as neovascular endothelial and malignant tumor cell models, respectively, to study the cellular association of nanoparticles. U87 MG tumor-bearing nude mice were applied to evaluate the biodistribution of CooP-NPs and the antitumor effect of CooP-NP-PTX.

RESULTS

Characterization of Nanoparticles. The sizes of NP-PTX were 109.76 ± 4.89 nm and slightly increased to 118.95 ± 7.36 nm after the modification with CooP peptide (Figure 1A,C and Table 1). A spherical morphology of both NP-PTX and CooP-NP-PTX was observed under TEM with no significant difference observed between NP-PTX and CooP-NP-PTX (Figure 1B,D). More importantly, the encapsulation of PTX

DOI: 10.1021/acs.bioconjchem.5b00379
Bioconjugate Chem. 2015, 26, 1850−1861

Table 1. Characterization of NP and CooP-NP (Data Represent Mean ± SD, n = 3)

nanoparticles	particle size (mean ± SD, nm)	polydispersity index (P.I.)	zeta potential (mV)
NP-PTX	109.76 ± 4.89	0.092 ± 0.023	−33.35 ± 3.46
CooP-NP-PTX	118.95 ± 7.36	0.157 ± 0.048	−27.59 ± 5.50

had no significant influence on particle size or morphology. The zeta potential of NP and CooP-NP was −33.35 ± 3.46 mv and −27.59 ± 5.50 mV, respectively.

As shown by XPS analysis, the percentage of nitrogen on the surface of CooP conjugated NP was 0.63% while that on the surface of unmodified NP was undetectable.

The EE of the optimized NP-PTX and CooP-NP-PTX was 47.07 ± 2.67% and 44 ± 3.15%, respectively, with the LC 1.49 ± 0.17% and 1.31 ± 0.26%, respectively.

In Vitro PTX Release. The release behavior of NP-PTX and CooP-NP-PTX was analyzed by HPLC. A similar release pattern was obtained for NP-PTX and CooP-NP-PTX (Figure 1E). After incubation for 96 h, 69.25% of PTX in NP-PTX and 73.52% of PTX in CooP-NP-PTX were released in the media of PBS (pH 7.4) containing 0.5% Tween 80. In the meanwhile, 82.91% of PTX in NP-PTX and 84.53% of PTX in CooP-NP-PTX were released in 10% rat plasma.

Expression of MDGI. Overexpression of MDGI in glioma was confirmed by staining with rabbit anti-MDGI antibodies. As shown in Figure 2, high expression of MDGI was detected in glioma, while an undetectable signal of MDGI was observed in normal brain tissue. The results indicated that MDGI as active targeting receptor might provide a promising way for glioma therapy.

Cellular Association of Nanoparticles in Cells. As shown in Figure 3A,B, cellular association of CooP-NP was significantly higher than unmodified NP at each determined concentration of nanoparticles (50 μg/mL, 100 μg/mL, 200 μg/mL, and 400 μg/mL).

To further assess cellular association of NP and CooP-NP, quantitative high content analysis system analysis was performed and the results confirmed the concentration and temperature dependent manner of nanoparticle uptake in HUVEC cells and U87MG cells (Figure 4A,C). In addition, time of incubation also played a pivotal role in the internalization of nanoparticles (Figure 4B,D). More importantly, no matter what kind of premise, cells treated with CooP-NP exhibited much stronger fluorescence intensity when compared with those treated with unmodified ones.

In the case of mechanism of cellular internalization of CooP-NP, results showed that the cellular uptake of CooP-NP was significantly inhibited by BFA (P < 0.001), filipin (P < 0.01), genistein (P < 0.001), NaN_3 (P < 0.001), M-β-CD (p < 0.01), and moneisin (p < 0.01) in HUVEC cells and colchicines (P < 0.01), cyto-D (P < 0.001), BFA (P < 0.001), filipin (P < 0.001), genistein (P < 0.01), M-β-CD (P < 0.01), and nocodazole (p < 0.001) in U87MG cells (Figure 5). In those cells pretreated with 100 μg CooP peptide, the association of CooP-NP was dramatically decreased by 70.57% (P < 0.001) and 71.83% (P < 0.001) on HUVEC cells and U87MG cells, respectively.

Cell Viability. Results of MTT assay revealed that CooP-NP-PTX exhibited higher antiproliferative ability compared with Taxol and NP-PTX (Figure 6). The IC_{50} value of Taxol, NP-PTX, and CooP-NP-PTX were 183.0, 149.1, and 71.47 ng/mL for HUVEC cells and 142.4, 119.3, and 54.45 ng/mL for U87MG cells, respectively. For the control group, cells treated with NP and CooP-NP exhibited an unconspicuous antiproliferation effect, indicating that the blank NP and Coop-NP possessed excellent cytocompatibility.

Cell Apoptosis Assay. For qualitative experiments, as shown in Figure 7A, no characteristic of nuclei apoptosis such as segmentation and fragmentation was observed in PTX free cells. In contrast, nuclei of those cells exposed to PTX formulations exhibited irregular shape and segmentation to varying degrees, with the group treated with CooP-NP-PTX exhibiting the greatest distribution of apoptotic bodies.

Annexin-V/PI double staining assay showed that CooP-NP-PTX induced the highest cellular apoptosis rate. The percentages of early and late apoptosis in the HUVEC cells treated with Taxol, NP-PTX, and CooP-NP-PTX were 6.43 ± 0.97% and 5.13 ± 1.44%, 7.47 ± 1.37% and 7.94 ± 2.10%, and 15.29 ± 1.79% and 7.51 ± 1.29%, respectively.

In Vivo Targeting of CooP-NP-DiR. Noninvasive NIR fluorescence imaging was performed to evaluate the targeting effect of CooP-NP-DiR in tumor-bearing nude mice. As displayed in Figure 8A,B, much stronger tumor-associated fluorescence intensity of CooP-NP-DiR was detected at the tumor site. The images of the main organs obtained from mice mentioned above further confirmed the tumor targeting of CooP-NP-DiR (Figure 8C,D).

In Vivo Tumor Distribution. Co-localization of tumor blood vessels, nuclei, and coumarin-6-labeled CooP-NP showed that CooP-NP exhibited not only a higher accumulation within the vascular but also a deeper penetration in the tumor parenchyma. In contrast, only weak fluorescence signals from NP were observed around blood vessel within tumor (Figure 9).

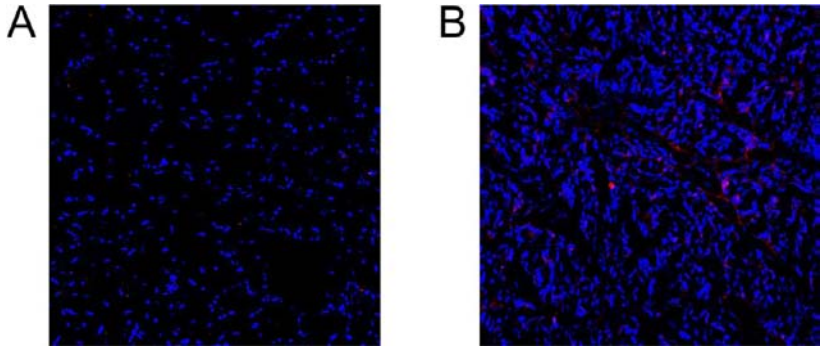

Figure 2. Expression of MDGI in normal brain section (A) and brain tumor section (B). Blue: DAPI stained cell nuclei. Red: Anti-goat Alexa 555.

DOI: 10.1021/acs.bioconjchem.5b00379
Bioconjugate Chem. 2015, 26, 1850−1861

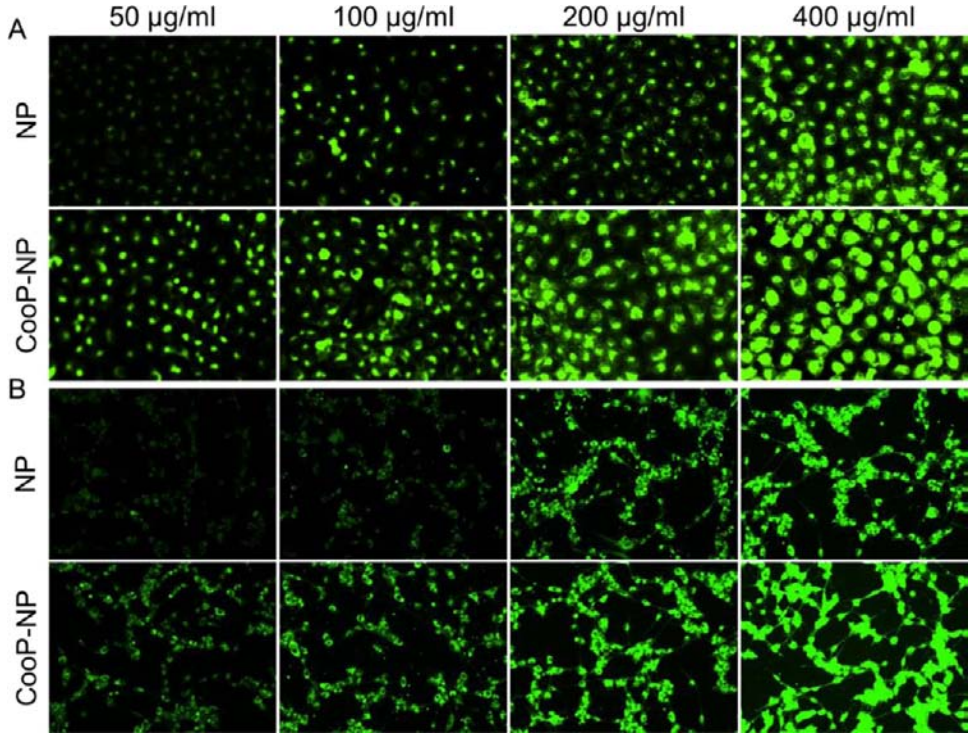

Figure 3. Qualitative measurement of cellular association of coumarin-6-labeled NP and CooP-NP in HUVEC cells (A) and U87 cells (B) after 1 h incubation at 37 °C at the detected concentrations: 50 μg/mL, 100 μg/mL, 200 μg/mL, and 400 μg/mL, respectively. Green: Coumarin-6-labeled nanoparticles. Original magnification: 20×.

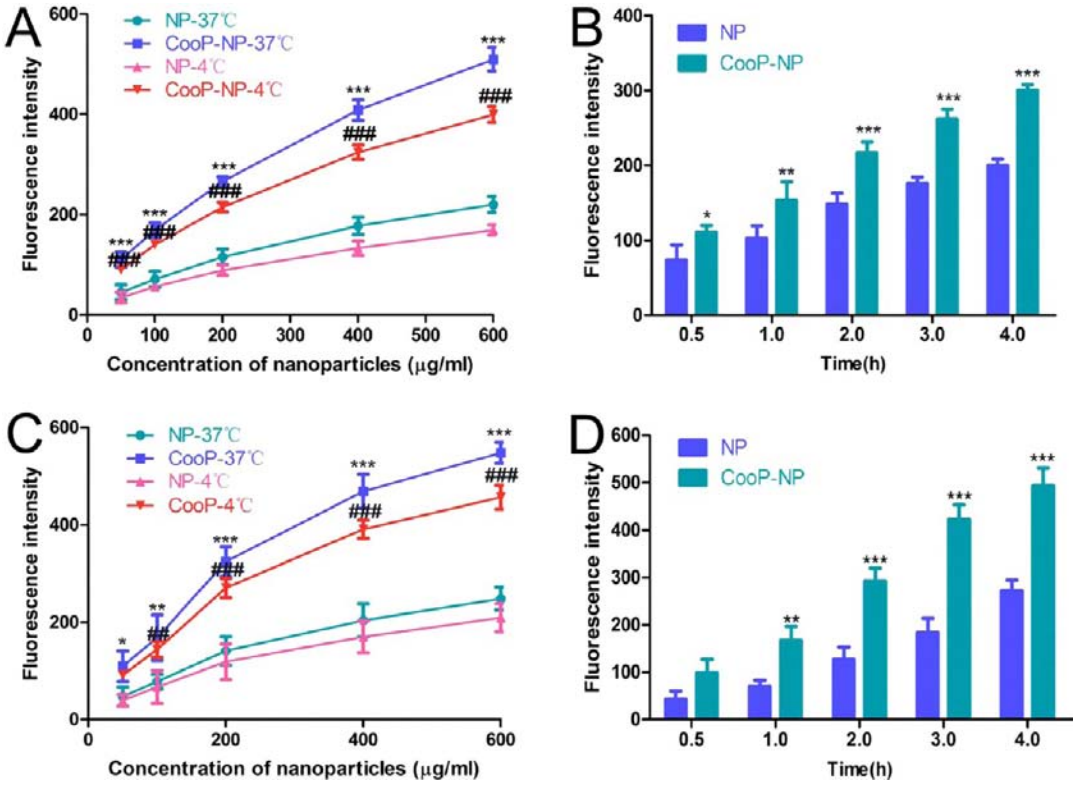

Figure 4. Quantitative measurement of cellular association of NP and CooP-NP in HUVEC cells (A) and U87 cells (C) at different concentrations of coumarin-6-labeled nanoparticles (from 50 μg/mL to 600 μg/mL) at 37 and 4 °C. Cellular association of NP and CooP-NP at different time points (0.5, 1 h, 2 h, 3 and 4 h) in HUVEC cells (B) and U87 cells (D) at the NPs concentration of 200 μg/mL. Data presented as mean ± SD (n = 3). *p < 0.05, **p < 0.01, ***p < 0.001 significantly higher than the cellular association of unmodified NP at 37 °C, and ##p < 0.01, ###p < 0.001 significantly higher than the cellular association of unmodified NP at 4 °C.

DOI: 10.1021/acs.bioconjchem.5b00379
Bioconjugate Chem. 2015, 26, 1850−1861

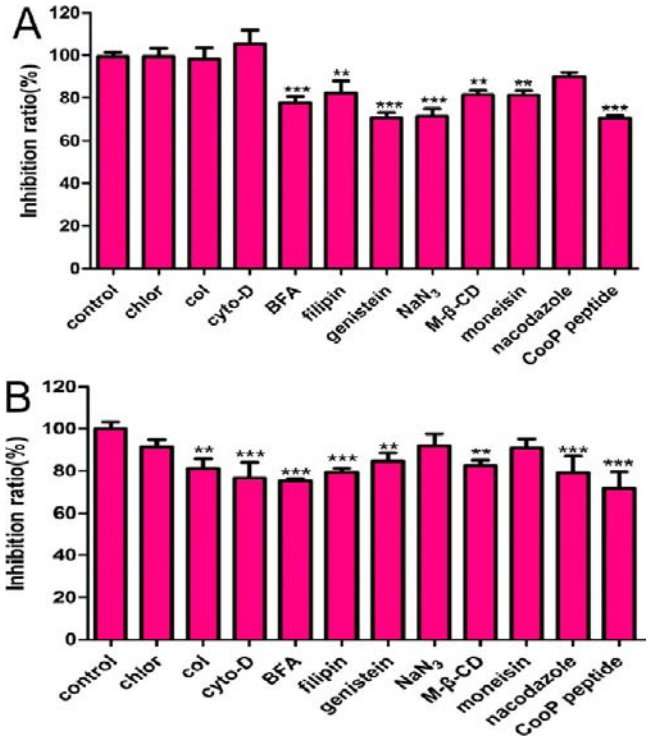

Figure 5. Cellular association of coumarin-6-labeled CooP-NP in HUVEC cells (A) and U87MG cells (B) in the presence of various endocytosis inhibitors. Fluorescence intensity of coumarin-6 in the noninhibited cells represented as the control. Date represented mean ± SD $^{**}p < 0.01$, $^{***}p < 0.001$ compared with control ($n = 3$).

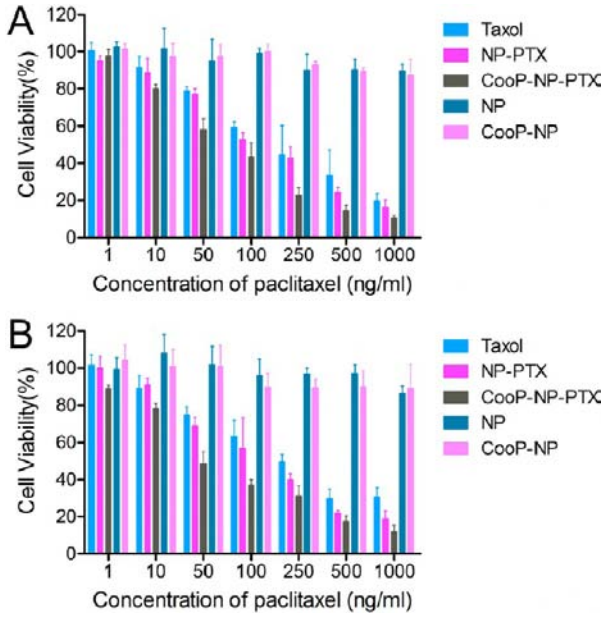

Figure 6. In vitro cell viability of HUVEC cells (A) and U87MG glioma cells (B) after treatment with Taxol, NP-PTX, CooP-NP-PTX, NP, and CooP-NP, respectively, for 48 h at 37 °C.

Antitumor Effect of CooP-NP in Vivo. The analysis of PTX-induced apoptosis in tumor neovasculature showed that a greater extent of vascular damage was induced by CooP-NP-PTX compared with that induced by Taxol and NP-PTX (Figure 10), manifesting that CooP-NP-PTX led to much greater apoptosis in endothelial cells.

For the evaluation of in vivo antitumor activity, various PTX formulations were injected into tumor bearing mice and the survival time of each was recorded. As shown in Figure 11B, the mice treated with CooP-NP-PTX exhibited the longest medium survival time (47.5 days), while those treated with saline, Taxol, and NP-PTX achieved the median survival time of 20, 25.5, and 29 days, respectively. The histopathologic changes of the PTX formulations treated mice were determined via an H&E staining assay. As shown in Figure 11C, CooP-NP-PTX induced much more apoptosis and necrosis in glioma cells than Taxol and NP-PTX.

DISCUSSION

Despite the emergence of various treatment modalities, gliomas still represent the most common and discouraging brain tumors.[26] As the highly aggressive and angiogenic form of glioma, glioblastoma multiform (GBM) might be the most difficult ones; individuals with it have a particularly poor prognosis and an average survival of less than two years.[27] Since angiogenesis plays a critical role in glioma development and growth, the formation of abnormal tumor vasculature is proposed to be one of the primary causes of glioma.[10,28] In addition, endothelial cells lining tumor blood vessels are directly accessible to drugs via the system circulation; anti-angiogenic therapy therefore has been recognized as a safe and effective method for tumor inhibition.[29]

A firm entry into oncology practice has been made by anti-angiogenic therapy in recent years, such as developed chemotherapeutics or therapeutic schedules including anti-body-based anti-angiogenic agents, anti-angiogenic drugs, and targeted therapies.[30−33] This seems mainly due to the rapid adaptation of tumors to antivascular therapy which will finally lead to tumor progression, metastasis, and increased vascular cooperation.[34−36] For the purpose of overcoming such difficulty, the ligand-based tumor cell and endothelial cell dual-targeting strategy has been recommended to suppress tumors more effectively.[37,38] However, such strategies rely on the identification of good-quality marks of pathology and on the isolation of high-affinity ligands with suitable pharmacokinetics.[39]

CooP peptide, with a highly selective specificity as a tumor homing peptide, was identified by in vivo phage technology as reported previously.[19] MDGI/FABP3, overexpressed in both glioma cells and vascular endotherial cells, has been recognized as the receptor that interacted with CooP. In this study, therefore, PEG−PLA nanoparticle-based drug delivery systems were prepared and modified with CooP peptide for targeting both glioma cells and vascular endotherial cells.

Since the physicochemical properties of nanoparticles have an important effect on its pharmacokinetics and bioavailability,[40] controlling the factors such as size and surface chemistry is of significance. The obtained unmodified nanoparticles in this study exhibited an average particle size of 105.76 ± 4.89 nm, which was in the optimal range for leveraging the EPR effect.[41] After the modification with CooP peptide, the size of the obtained nanoparticles slightly increased to 116.95 ± 7.36 nm. In addition, the fully hydrophilic PEG on the surface of CooP-NP could significantly reduce serum protein binding and greatly prolong the circulation times of the nanoparticles.[42]

The dual-targeting effect of CooP-NP depended on the specific interaction between CooP and MDGI; hence, the pivotal role of high expression of MDGI in tumor was

DOI: 10.1021/acs.bioconjchem.5b00379
Bioconjugate Chem. 2015, 26, 1850−1861

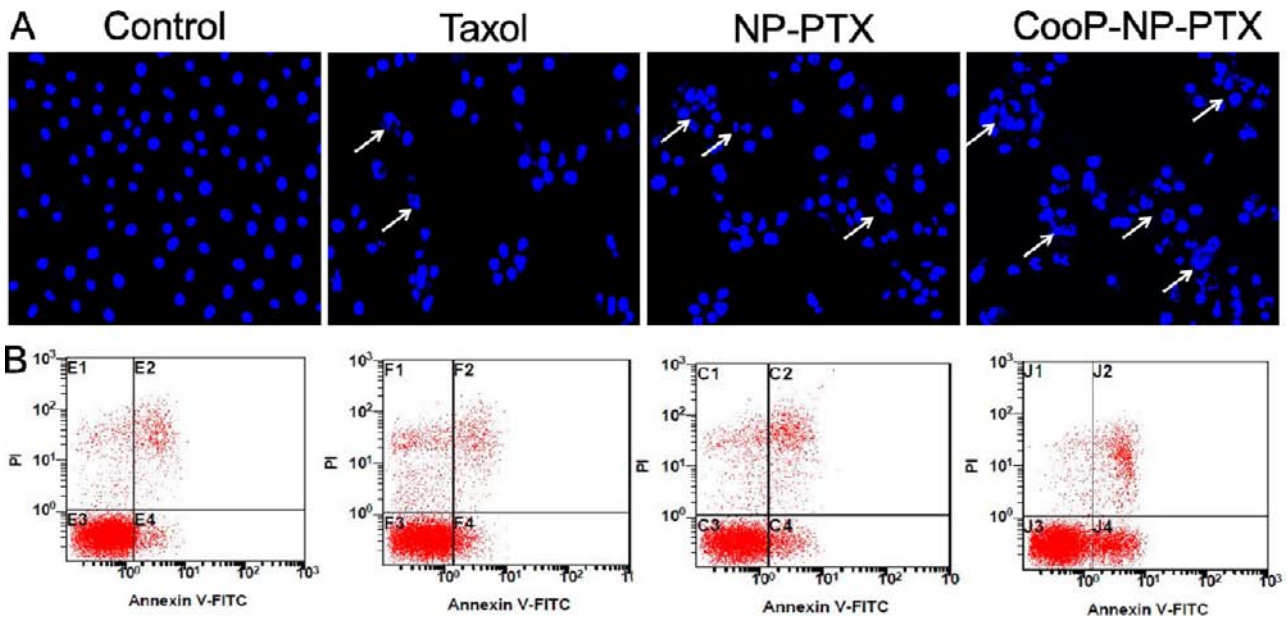

Figure 7. Apoptosis induced by various PTX formulations in HUVEC cells after 24 h incubation. (A) Fluorescence micrographs of HUVEC cell nuclei labeled by Hoechst 33258. (B) Flow cytometry used staining of Annexin V-FITC and PI. Cells incubated with drug-free DMEM served as the control. Arrows indicated cell apoptosis. Original magnification: 20×.

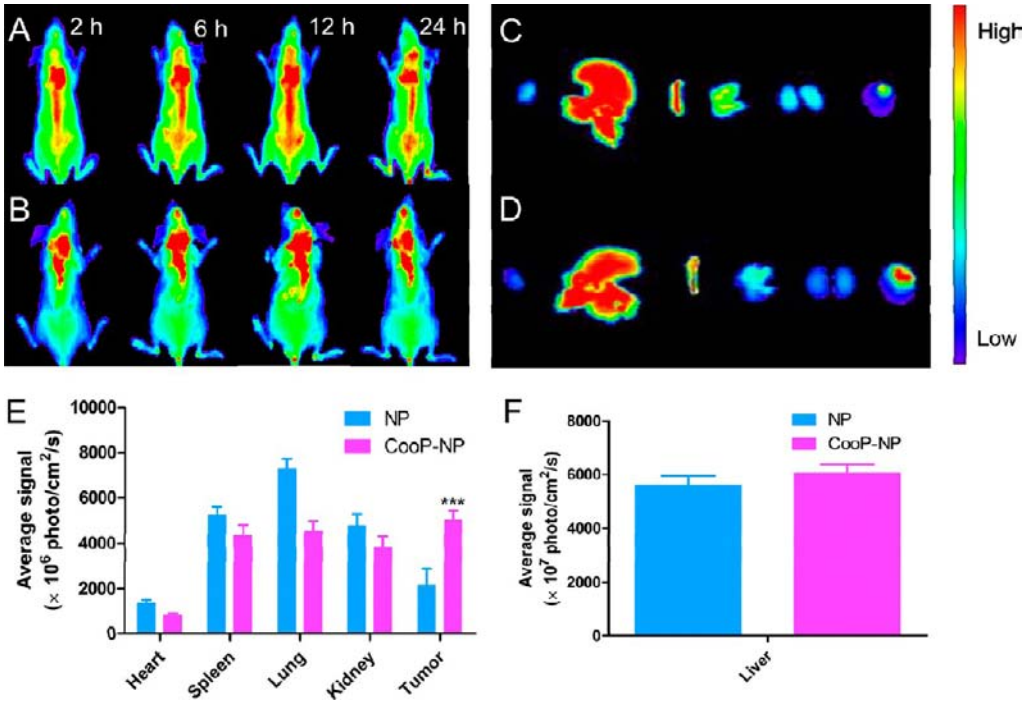

Figure 8. In vivo imaging of DiR-labeled NP (A,C) and CooP-NP (B,D) in U87MG tumor-bearing nude mice and dissected organs. For semiquantitative interpretation of the intensity in various organs and tumor, the data are presented as the mean ± SD (n = 3) (E,F), ***P < 0.001 vs NP.

highlighted. As shown in Figure 2, overexpression of MDGI was observed in glioma, while negligible signal was detected in the normal brain. Cellular uptake experiments were performed on U87MG cells and HUVEC cells to examine the dual-targeting efficiency of CooP-NP in vitro. Results indicated that the fluorescence intensity of CooP-NP was significantly higher than that of NP (Figures 3 and 4), and the enhanced cellular association of nanoparticles led to higher antiproliferation activity and enhanced ability of PTX-induced cell apoptosis in HUVEC cells and U87MG cells as demonstrated by MTT assay and Annexin-V/PI double staining assay.

Various endocytosis inhibitors were introduced to study the mechanism of cellular uptake of CooP-NP in HUVEC cells and U87MG cells.[43] Results shown in Figure 5A indicated that the association of CooP-NP in HUVEC cells and U87MG cells was both energy-dependent and caveolae-mediated. Besides, Golgi apparatus and lipid rafts were also involved in the endocytosis process. As manifested in this study, lysosome inhibitor

DOI: 10.1021/acs.bioconjchem.5b00379
Bioconjugate Chem. 2015, 26, 1850−1861

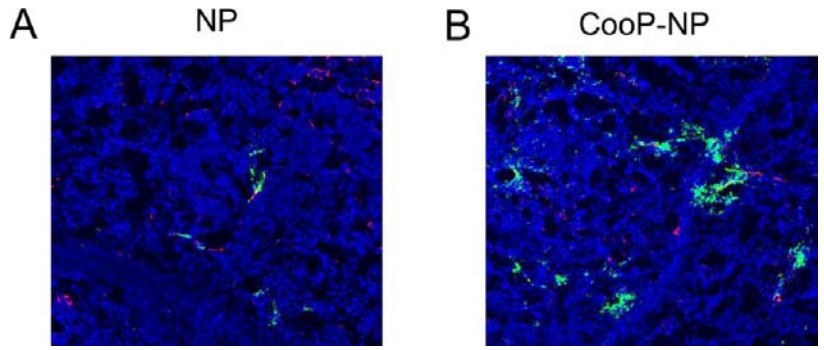

Figure 9. Distribution of coumarin-6 labeled NP and CooP-NP in the brains of glioma-bearing mice 3 h after injection. Red: anti-CD31 stained blood vessels. Blue: DAPI stained cell nuclei. Green: coumarin-6 labeled NP.

monensin significantly restricted the CooP-NP uptake in HUVEC cells but exhibited no effect in U87MG cells. In addition, the cellular uptake of CooP-NP in U87MG cells was inhibited by microtubule depolymerization agent nocodazole and colchicines, indicating microtubules were indispensable in the endocytosis pathway. Importantly, the association of CooP-NP in both cells significantly decreased once the cells were pretreated with CooP peptide, which further confirmed that interaction between CooP and MDGI facilitated the cellular uptake of CooP-NP in both HUVEC cells and U87MG cells.

Considering that the process of nanoparticle-mediated drug delivery to tumor through blood circulation is complicated and the resultant effect might be modestly ascribed to many factors in the blood such as macrophages,[44] in vivo targeting efficacy and glioma accumulation capacity of CooP-NP were evaluated here. It was found that compared with unmodified NPS, CooP-NP exhibited a higher accumulation in tumor but a lower aggregation in normal tissues (Figure 8A and B). Such selective accumulation of CooP-NP in tumor was further confirmed by the ex vivo imaging (Figure 8C and D), indicating that the interaction between CooP and MDGI contributed to a significant superiority in tumor targeting. The therapeutic effect of CooP-NP-PTX on glioma-bearing mice was further evaluated, in which in vivo anti-angiogenesis revealed that CooP peptide-mediated dual-targeting drug delivery destroyed the blood vessels to the greatest extent. As a result, the median survival time of those mice treated with CooP-NP-PTX was significantly prolonged (2.38-, 1.86-, and 1.64-fold longer than that following the treatment of saline, Taxol, and NP-PTX). In conclusion, the CooP peptide functionalized nanoparticles prepared in the present study could efficiently and precisely deliver chemotherapeutics to tumor, and might therefore provide an efficient method for tumor therapy.

CONCLUSION

A CooP peptide surface-modified PEG−PLA-based nanoparticulate drug delivery system was developed in this study. In vitro cellular experiments justified the dual targeting effect of CooP-NP in HUVEC cells and U87MG cells. In vivo imaging assay found that, compared with unmodified NP, CooP-NP displayed a significantly stronger fluorescence intensity at the tumor site. More importantly, pharmacodynamics analysis showed that the mice treated with CooP-NP-PTX achieved the longest median survival time. These findings together indicated that CooP-NP, an effective tumor angiogenic blood vessel and glioma cell dual-targeting nanocarrier, holds great potential to improve anticancer activity and avoid the drawbacks of anti-angiogenic therapy alone.

MATERIALS AND METHODS

Materials. Methoxy poly(ethylene glycol) $_{3000}$-poly(lactic acid) $_{34000}$ (MePEG−PLA) and maleimide-poly(ethylene glycol) $_{3400}$-poly(lactic acid) $_{34000}$ (Male−PEG-PLA) were kindly provided by East China University of Science and Technology. Coumarin-6, DiR (1,1′-dioctadecyl-3,3,3′,3′-tetramethyl indotricarbocyanine Iodide) and Hoechst 33258 were provided by Biotium (Hayward, CA). DAPI (4,6-diamidino-2-phenylindole) was purchased from Molecular Probes (Eugene, OR, USA), Hoechst 33258, and 3-[4,5-dimethylthiazol-2-yl]-2,5-diphenyl tetrazolium bromide (MTT) were all purchased from Sigma-Aldrich (St. Louis, MO, USA). PTX was obtained from Xi'an Sanjiang Biological Engineering Co. Ltd. (Xi'an, China) and Taxol was from Bristol-Myers Squibb Company. Alexa Fluor 555 goat anti-rabbit antibody and rabbit anti-MDGI antibody were purchased from Life Technology and Santa Cruz Biotechnology, respectively (USA). Alexa Fluor 594 anti-mouse CD31 Antibody was purchased from Biolegend. Growth factor-reduced Matrigel matrix and Annexin V-FITC Apoptosis Detection Kit I were purchased from BD Bioscience (San Diego, CA, USA). All the other solvents were purchased from Sinopharm Chemical Reagent Co., Ltd. (Shanghai, China) and were of analytical or chromatographic grade.

CooP peptide (ACGLSGLGVA) was synthesized by Shanghai GL Biotech Co, Ltd. (Shanghai, China). Dulbecco's Modified Eagle Medium (DMEM) (high glucose) cell culture medium, certified fetal bovine serum (FBS), penicillin/streptomycin stock solutions, and 0.25% Trypsin-EDTA were all obtained from Invitrogen Co, USA.

Cells and Animals. Primary human umbilical vein endothelial cells (HUVEC) were purchased from Cascade Biologics (USA); U87MG glioblastoma cell was obtained from Cell Institute of Chinese Academy of Sciences (Shanghai, China). Both of those cells were cultured in DMEM containing 10% fetal bovine serum, 100 U/mL penicillin, and 100 μg/mL streptomycin at 37 °C in a 5% CO_2/95% air humidified environment incubator (Thermo HERAcell, USA).

Balb/c nude mice (male, 20 ± 2 g) were obtained from Experimental Animal Center of Fudan University and housed at 25 ± 1 °C with access to food and water. The protocol of animal experiments was approved by the Animal Experimentation Ethics Committee of Fudan University.

Preparation of Nanoparticles. PEG−PLA nanoparticles loaded with PTX were prepared through the technique of

DOI: 10.1021/acs.bioconjchem.5b00379
Bioconjugate Chem. 2015, 26, 1850−1861

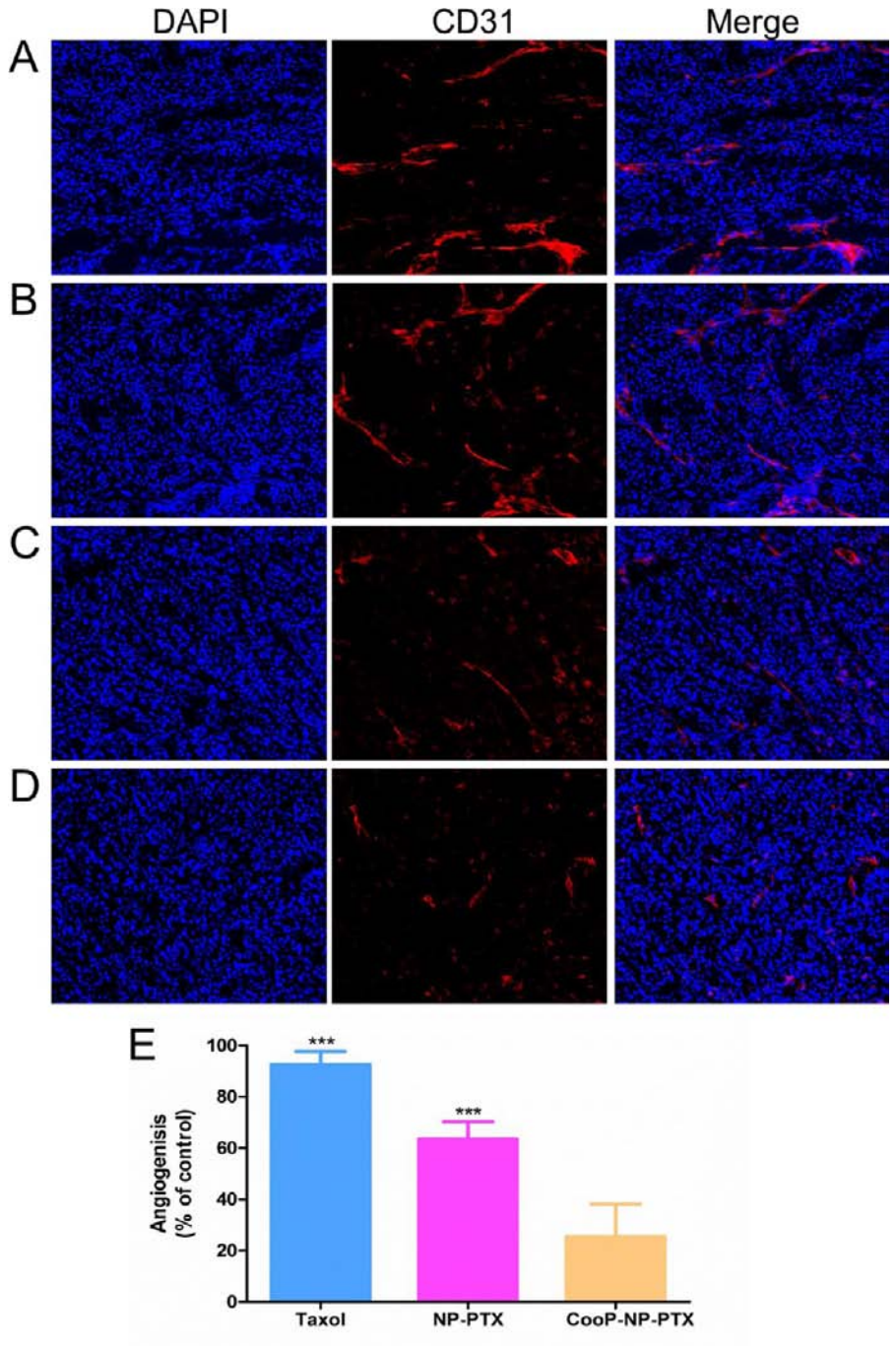

Figure 10. In vivo antiangiogenesis effect induced in those mice treated with Taxol (B), NP-PTX (C), and CooP-NP-PTX (D), respectively. The mice administrated with saline server as the control (A). Quantitative data represented as percentages of the control group (E), ***$p < 0.001$. Red: anti-CD31 antibody stained blood vessel. Blue: DAPI stained nuclei.

emulsion/solvent evaporation as described elsewhere.[45] Briefly, MePEG−PLA (22.5 mg), Male−PEG-PLA (2.5 mg), and PTX (0.5 mg) were dissolved in 1 mL of dichloromethane, 2 mL of 1% sodium cholate was then added and emulsified by sonication (280 w, 30 s) under the condition of ice bath using probe sonicator (Ningbo Scientz Biotechnology Co. Ltd., China). The emulsion was further diluted into 8 mL of 0.5% sodium cholate aqueous solution and stirred for 5 min with uniform velocity under rapid magnetic stirring. After that, a rotary evaporator (Shanghai Institute of Organic Chemistry, China) was applied to rapidly eliminate the dichloromethane. The unmodified NP-PTX was obtained by discarding the supematant by centrifugation at 14 500 rpm using a TJ-25 centrifuge (Beckman Counter, USA) at 4 °C for 1 h and was kept at 4 °C for further use.

Fluorescein-labeled nanoparticles were prepared with the same procedure as mentioned above except that PTX was replaced with Coumarin-6 and DiR. CooP modified nanoparticles were prepared via a maleimide−thiol coupling reaction at room temperature for 6 h. The products were then eluted with 0.01 M HEPES buffer (pH 7.0) and through a 1.5 × 20 cm Sepharose CL-4B column to remove the unconjugated peptide.

Characterization of Nanoparticles. Particle size and zeta potential of PTX-loaded NP (NP-PTX) and PTX-loaded

DOI: 10.1021/acs.bioconjchem.5b00379
Bioconjugate Chem. 2015, 26, 1850−1861

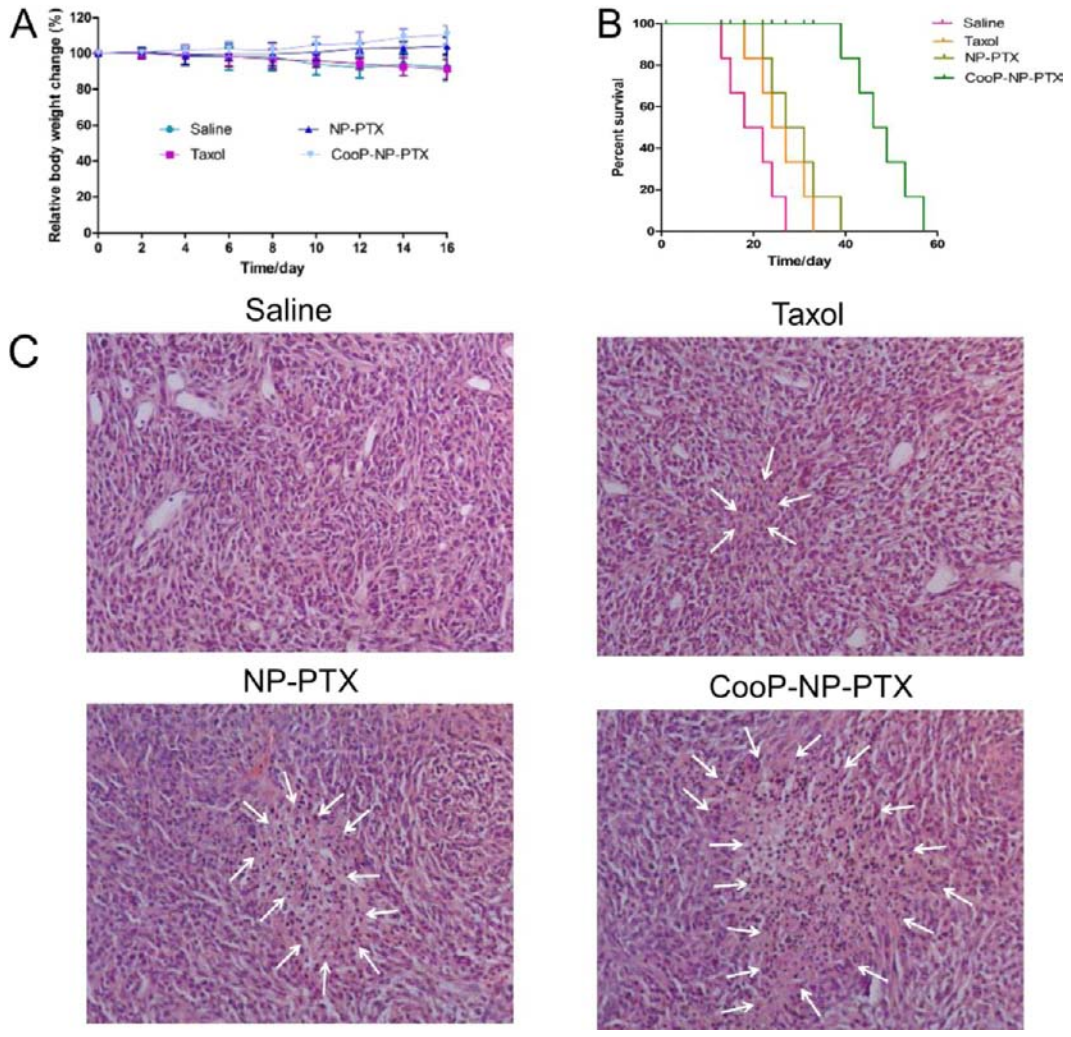

Figure 11. Antitumor efficacy of Taxol, NP-PTX, CooP-NP-PTX (PTX dose of 5 mg/kg) and saline, respectively. (A) Changes in body weights of mice after treatment. (B) Kaplan−Meier survival curve of tumor bearing mice. (C) H&E staining of glioma tissue sections. Data represents mean ± SD, $n = 6$.

CooP-NP (CooP-NP-PTX) were determined by dynamic light scattering detector (Zetasizer, Nano-ZS, Malvern, UK). The morphological examination of NPs was performed via a transmission electron microscope (TEM) (H-600, Hitachi, Japan).

To verify the modification of CooP peptide on the surface of nanoparticles, the NP samples were lyophilized via an ALPHA 2−4 Freeze-Dryer (0.070 Mbar Vacuum, −80 °C, Martin Christ, Germany) and then subjected to X-ray photoelectron spectroscopy (XPS) analysis via a RBD upgraded PHI-5000C ESCA system (PerkinElmer) to determine the surface composition.

To determine the encapsulation efficiency (EE) and loading capacity (LC) of PTX in NP-PTX and CooP-NP-PTX, the NP samples were dissolved in acetonitrile and subsequently analyzed on an Agilent 1100 HPLC system (Agilent Technologies, CA, USA) with the detection wavelength of 227 nm.[45] The encapsulation efficiency (EE) and loading capacity (LC) were calculated as indicated below ($n = 3$).

$$\mathrm{EE}(\%) = \frac{\text{Amount of PTX in the nanoparticles}}{\text{Total amount of PTX added}} \times 100\%$$

$$\mathrm{LC}(\%) = \frac{\text{Amount of PTX in nanoparticles}}{\text{nanoparticles weight}} \times 100\%$$

In Vitro PTX Release. The release of PTX from NP-PTX and CooP-NP-PTX was measured in vitro via the equilibrium dialysis method described previously.[46] PBS (pH 7.4) with 0.5% (v/v) Tween-80 and 10% rat plasma were used as release media, respectively, under a pseudosink condition. One milliliter of the freshly prepared NP-PTX and CooP-NP-PTX (containing 0.1 mg PTX) was added into the dialysis bag (MWCO = 8000 Da, Greenbird Inc., Shanghai, China) with the end sealed and incubated in 30 mL release medium at 37 °C at a shaking speed of 120 rpm for 96 h. Then, 0.2 mL aliquots of sample were withdrawn at predetermined time points and the concentration of PTX was analyzed through HPLC as described elsewhere.[47]

Detection of MDGI Expression. The U87MG tumor-bearing nude mice model was established as described elsewhere.[45] In brief, trypsinized U87MG cells were suspended in PBS (pH 7.4, 5×10^5 cells/5 μL) and the cell suspension was injected into right corpus striata of nude mice using a stereotaxic apparatus, with these mice cultured for 2 weeks under the standard condition.

DOI: 10.1021/acs.bioconjchem.5b00379
Bioconjugate Chem. 2015, 26, 1850−1861

The expression of MDGI in glioma cells and normal tissues was identified through an immunofluoresent assay.[24] Briefly, the U87 MG tumor-bearing mice and normal mice were perfused with saline and 4% paraformaldehyde, then the brains harvested and fixed by 4% paraformaldehyde and dehydrated with sucrose solutions (10% and 30% sucrose solution). To visualize MDGI, sections were stained with rabbit anti-MDGI antibodies followed by Alexa555-conjugated second antibodies and then subjected to DAPI staining for nuclear positioning. Finally, sections were examined under a Zeiss LSM 510 confocal microscope.

Cellular Association of Nanoparticles. Both U87MG cells and HUVEC cells were seeded in 96-well plates at the density of 5000 cells per well. On the second day, the cells have attached tightly within the plates. Then, fresh serum-free DMEM containing coumarin-6-labeled NP and CooP-NP was added into those wells at the concentrations of nanoparticles ranging from 50 to 400 μg/mL. One hour later, nanoparticle suspension was removed and washed with ice-cold PBS. Subsequently, cells were fixed with 4% paraformaldehyde and preserved by 200 μL PBS for qualitative imaging under a fluorescent microscopy (Leica DMI4000 B, Germany).

For quantitative analysis, U87MG cells and HUVEC cells were incubated with coumarin-6-labeled NP and CooP-NP (50−600 μg/mL) for 1 h at 4 and 37 °C, respectively. After that, the cells were washed twice with PBS and fixed with 4% paraformaldehyde solution for 15 min. After staining with 2 μg/mL Hochest 33258 at room temperature for 10 min, the cells were then subjected to detection under a KineticScan HCS Reader (version 3.1, Cellomics Inc., Pittsburgh, PA, USA). To evaluate the role of incubation time in CooP-NP uptake by HUVEC cells and U87MG cells, both cells were coincubated with 200 μg/mL nanoparticles for 0.5, 1, 2, and 4 h at 37 °C, respectively.

To explore the mechanism of cellular internalization of CooP-NP, endocytosis inhibition experiments were performed. U87MG cells and HUVEC cells were seeded in 96-well plates at the density of 5000 cells per well. Twenty-four hours later, the cells were incubated with endocytic inhibitors including 10 μg/mL chlorpromazine, 4 μg/mL colchicines, 10 μg/mL cyto-D, 5 μg/mL BFA, 5 μg/mL filipin, 2.5 μg/mL genistein, 10 mM NaN_3, 2.5 mM methyl-β-cyclodextrin (M-β-CD), 200 nM monensin, 20 μM nocodazole, and 200 μg/mL CooP peptide for 1 h, respectively, and then incubated with coumarin-6-labeled CooP-NP at the concentration of 200 μg/mL for 1 h at 37 °C. After that, quantitative analysis of cellular association of the nanoparticles was performed as described above.

Antiproliferation Assay. U87MG cells and HUVEC cells were seeded in 96-well plates at the density of 5000 cells per well and allowed to attach overnight. After removal of the primary medium, 200 μL fresh serum-free medium containing Taxol, NP-PTX, and CooP-NP-PTX at the PTX concentration ranging from 1 ng/mL to 1000 ng/mL were added. Cells incubated with PTX-free NP and CooP-NP (with concentrations from 1 ng/mL to 1 μg/mL) were applied as the negative control. After 48 h incubation, 20 μL MTT solutions (5 mg/mL) were added into those wells and coincubated with cells for another 4 h at 37 °C, and then the formation of formazan crystals was dissolved through addition of 150 μL DMSO. After being gently shaken for 10 min away from light, cells were subjected to microplate reader (Thermo Multiskan MK3, USA) at wavelength of 570 nm.

Cell Apoptosis Assay. To evaluate the endothelial cell apoptosis induced by various PTX formulations, qualitative and quantitative experiments on HUVEC cells were carried out. For qualitative analysis, cells were seeded in 24-well plates at the density of 2×10^5 cells per well. After culturing for 24 h at 37 °C, cells were treated with various PTX formulations including Taxol, NP-PTX, and CooP-NP-PTX at the PTX concentration of 100 ng/mL for 48 h. Then, the cells were fixed with 4% paraformaldehyde solution for 15 min, washed twice with PBS, stained with DAPI, and then subjected to observation under a fluorescent microscope (Leica DMI4000 B, Germany).

For quantitative analysis, HUVEC cells were seeded in 6-well plates at the density of 5 × 105 cells per well. Twenty-four hours later, the cells were coincubated with Taxol, NP-PTX, and CooP-NP-PTX at the PTX concentration of 100 ng/mL, respectively, for 24 h. After that, the cells were trypsinized, centrifuged at 1000 g for 5 min, and resuspended in 200 μL binding buffer for double staining with Annexin V-FITC (5 μL) and PI (10 μL) according to the manufacturer's protocol. The stained cells were then analyzed via a flow cytometer (FACSCalibur, BD, USA). For both qualitative and quantitative analysis, cells treated with DMEM were served as control.

In Vivo Imaging of CooP-NP-DiR. The tumor bearing mice were randomly divided into two groups and intravenously administrated with 200 μL of DiR-loaded NP or CooP-NP (1 mg/kg). The fluorescent images were acquired using an In Vivo IVIS spectrum imaging system (PerkinElmer, USA) at predetermined time point (2, 6, 12, and 24 h) after injection. After 24 h post-injection, the mice were sacrificed with the brains and other principle organs (including heart, liver, spleen, lung, and kidney) harvested and imaged.

Distribution of Coumarin-6-Labeled CooP-NP in Tumor. Nude mice bearing intracranial glioma were established as mentioned above and intravenously administered coumarin-6-loaded NPs or CooP-NP (n = 3). Three hours post-injection, the mice were anesthetized and hearts perfused with saline and 4% paraformaldehyde. Then, the collected brains were sectioned (10 μm) for further measurement after procedures as described above. For analysis, the sections were stained with anti-mouse CD31 followed by Alexa 594 conjugated secondary antibodies to visualize the tumor blood vessel and DAPI was used for nuclei staining. Finally, the sections were examined under a Zeiss LSM 510 confocal microscope.

Examining Destruction of Angiogenesis in Tumor Post-Treated with PTX Formulations. To evaluate the destruction of angiogenesis induced by PTX formulations, tumor bearing mice were administered with Taxol, NP-PTX, and CooP-NP-PTX at PTX dose of 5 mg/kg. Meanwhile, mice treated with saline were used as the control. One week later, tumor brains were removed and cryostat sections were prepared. Sections were stained with Alexa 594 to visualize tumor angiogenesis as described above and treated with DAPI for nuclei staining. Finally, sections were examined by the Zeiss LSM 510 confocal microscope.

In Vivo Antitumor Efficacy. To study the therapeutic effect of CooP-NP-PTX, glioma bearing mice were randomly divided into four groups (n = 6) and treated with saline, Taxol, NP-PTX, and CooP-NP-PTX (PTX concentration of 5 mg/kg), respectively. Every 3 days in 2 weeks mice in each group were repeatedly treated with various PTX formulations and saline, and then the survival time of each group was monitored and analyzed. The relative body weight change at predeter-

DOI: 10.1021/acs.bioconjchem.5b00379
Bioconjugate Chem. 2015, 26, 1850−1861

mined times was recorded. After that, the brains were harvested and fixed by 10% neutral formalin at least for 48 h followed by H&E staining.[48]

Statistical Analysis. All the data were presented as mean ± SD unless otherwise indicated. Comparison among the different groups was performed by one-way ANOVA followed by Bonferroni tests. $p < 0.05$ was considered to be significant.

AUTHOR INFORMATION

Corresponding Authors

*E-mail: jyliang@shmu.edu.cn. Tel.: +86-21-51980056.
*E-mail: chenjun@fudan.edu.cn. Tel.: +86-21-51980066. Fax: +86 21 51980069.

Author Contributions

The first two authors contributed equally to this work.

Notes

The authors declare no competing financial interest.

ACKNOWLEDGMENTS

This work was supported by National Natural Science Foundation of China (81373353), National Key Basic Research Program (2013CB932500), Grants from Shanghai Science and Technology Committee (13NM1400500) and Program for New Century Excellent Talents in University (NCET-12-0130).

REFERENCES

(1) Furnari, F. B., Fenton, T., Bachoo, R. M., Mukasa, A., Stommel, J. M., Stegh, A., Hahn, W. C., Ligon, K. L., Louis, D. N., Brennan, C., et al. (2007) Malignant astrocytic glioma: genetics, biology, and paths to treatment. *Genes Dev. 21*, 2683−2710.

(2) Louis, D. N., Ohgaki, H., Wiestler, O. D., et al. (2007) The 2007 WHO Classification of Tumors of the Central Nervous System. *Acta Neuropathol. 114*, 97−109.

(3) Kim, W. Y., and Lee, H. Y. (2009) Brain angiogenesis in developmental and pathological processes: mechanism and therapeutic intervention in brain tumors. *FEBS J. 276*, 4653−4664.

(4) Newton, H. B. (2006) Advances in strategies to improve drug delivery to brain tumors. *Expert Rev. Neurother. 6*, 1495−1509.

(5) Raza, S. M., Pradilla, G., Legnani, F. G., Thai, Q. A., Olivi, A., Weingart, J. D., and Brem, H. (2005) Local delivery of antineoplastic agents by controlled-release polymers for the treatment of malignant brain tumors. *Expert Opin. Biol. Ther. 5*, 477−94.

(6) Weis, S. M., and Cheresh, D. A. (2011) Tumor angiogenesis: molecular pathways and therapeutic targets. *Nat. Med. 17*, 1359−70.

(7) Semenza, G. L. (2010) Defining the role of hypoxia-inducible factor 1 incancer biology and therapeutics. *Oncogene 29*, 625−34.

(8) Ellis, L. M., and Hicklin, D. J. (2008) VEGF-targeted therapy: mechanisms of anti-tumour activity. *Nat. Rev. Cancer 8*, 579−91.

(9) Vajkoczy, P., Schilling, L., Ullrich, A., Schmiedek, P., and Menger, M. D. (1998) Characterization of angiogenesis and microcirculation of high-grade glioma: an intravital multi-fluorescence microscopic approach in the athymic nude mouse. *J. Cereb. Blood Flow Metab. 18*, 510−20.

(10) Bello, L., Giussani, C., Carrabba, G., Pluderi, M., Costa, F., and Bikfalvi, A. (2004) Angiogenesis and invasion in gliomas. *Cancer Treat Res. 117*, 263−284.

(11) Tubin, S., Valeriani, M., Salerno, G., Bracci, S., Stoppacciaro, A., Cardelli, P., Osti, M. F., De Sanctis, V., Minniti, G., and Maurizi Enrici, R. (2015) Manipulation of radiation-induced bystander effect in prostate adenocarcinoma by dose and tumor differentiation grade: In vitro study. *Int. J. Radiat. Biol. 91*, 166−171.

(12) Bai, F., Wang, C., Lu, Q., Zhao, M., Ban, F. Q., Yu, D. H., Guan, Y. Y., Luan, X., Liu, Y. R., Chen, H. Z., and Fang, C. (2013) Nanoparticle-mediated drug delivery to tumor neovasculature to combat P-gp expressing multidrug resistant cancer. *Biomaterials 34*, 6163−74.

(13) Pàez-Ribes, M., Allen, E., Hudock, J., Takeda, T., Okuyama, H., Viñals, F., Inoue, M., Bergers, G., Hanahan, D., and Casanovas, O. (2009) Antiangiogenic therapy elicits malignant progression of tumors to increased local invasion and distant metastasis. *Cancer Cell 15*, 220−31.

(14) Gabrusiewicz, K., Liu, D., Cortes-Santiago, N., Hossain, M. B., Conrad, C. A., Aldape, K. D., Fuller, G. N., Marini, F. C., Alonso, M. M., Idoate, M. A., et al. (2014) Anti-vascular endothelial growth factor therapy-induced glioma invasion is associated with accumulation of Tie2-expressing monocytes. *Oncotarget. 5*, 2208−20.

(15) Ebos, J. M., Lee, C. R., Cruz-Munoz, W., Bjarnason, G. A., Christensen, J. G., and Kerbel, R. S. (2009) Accelerated Metastasis after Short-Term Treatment with a Potent Inhibitor of Tumor Angiogenesis. *Cancer Cell 15*, 232−9.

(16) de Groot, J. F., Fuller, G., Kumar, A. J., Piao, Y., Eterovic, K., Ji, Y., and Conrad, C. A. (2010) Tumor invasion after treatment of glioblastoma with bevacizumab: radiographic and pathologic correlation in humans and mice. *Neuro Oncol. 12*, 233−242.

(17) Keunen, O., Johansson, M., Oudin, A., Sanzey, M., Rahim, S. A., Fack, F., Thorsen, F., Taxt, T., Bartos, M., Jirik, R., et al. (2011) Anti-VEGF treatment reduces blood supply and increases tumor cell invasion in glioblastoma. *Proc. Natl. Acad. Sci. U. S. A. 108*, 3749−54.

(18) Pastorino, F., Brignole, C., Di Paolo, D., Nico, B., Pezzolo, A., Marimpietri, D., Pagnan, G., Piccardi, F., Cilli, M., Longhi, R., et al. (2006) Targeting liposomal chemotherapy via both tumor cell-specific and tumor vasculature-specific ligands potentiates therapeutic efficacy. *Cancer Res. 66*, 10073−82.

(19) Hyvönen, M., Enbäck, J., Huhtala, T., Lammi, J., Sihto, H., Weisell, J., Joensuu, H., Rosenthal-Aizman, K., El-Andaloussi, S., Langel, U., et al. (2014) Novel target for peptide-based imaging and treatment of brain tumors. *Mol. Cancer Ther. 13*, 996−1007.

(20) Huynh, H., Alpert, L., and Pollak, M. (1996) Silencing of the Mammary-derived Growth Inhibitor (MDGI) Gene in Breast Neoplasms Is Associated with Epigenetic Changes. *Cancer Res. 56*, 4865−4870.

(21) Nevo, J., Mattila, E., Pellinen, T., Yamamoto, D. L., Sara, H., Iljin, K., Kallioniemi, O., Bono, P., Heikkilä, P., Joensuu, H., Wärri, A., and Ivaska, J. (2009) Mammary-Derived Growth Inhibitor Alters Traffic of EGFR and Induces a Novel Form of Cetuximab Resistance. *Clin. Cancer Res. 15*, 6570−81.

(22) Storch, J., and Corsico, B. (2008) The emerging functions and mechanisms of mammalian fatty acid-binding proteins. *Annu. Rev. Nutr. 28*, 73−95.

(23) Wang, H. L., and Kurtz, A. (2000) Breast cancer growth inhibition by delivery of the MDGI-derived peptide P108. *Oncogene 19*, 2455−60.

(24) Kinnari, P. J., Hyvönen, M. L., Mäkilä, E. M., Kaasalainen, M. H., Rivinoja, A., Salonen, J. J., Hirvonen, J. T., Laakkonen, P. M., and Santos, H. A. (2013) Tumor homing peptide-functionalized porous silicon nanovectors for cancer therapy. *Biomaterials 34*, 9134−9141.

(25) Hyvönen, M., Virtanen, J., Rivinoja, A., Enbäck, J., Joensuu, H., Mari, B., Tavi, F., Lehti, K., and Laakkonen, P. (2012) The role of MDGI in glioma progression. *Eur. J. Cancer 48*, 52−53.

(26) Arismendi-Morillo, G. (2011) Electron microscopy morphology of the mitochondrial network in gliomas and their vascular microenvironment. *Biochim. Biophys. Acta, Bioenerg. 1807*, 602−8.

(27) Kanamori, M., Kawaguchi, T., Berger, M. S., and Pieper, R. O. (2006) Intracranial Microenvironment Reveals Independent Opposing Functions of Host $\alpha V\beta 3$ Expression on Glioma Growth and Angiogenesis. *J. Biol. Chem. 281*, 37256−64.

(28) Cea, V., Sala, C., and Verpelli, C. (2012) Antiangiogenic Therapy for Glioma. *J. Signal Transduction 2012*, 1−15.

(29) Hajitou, A., Pasqualini, R., and Arap, W. (2006) Vascular Targeting: Recent Advances and Therapeutic Perspectives. *Trends Cardiovasc. Med. 16*, 80−88.

DOI: 10.1021/acs.bioconjchem.5b00379
Bioconjugate Chem. 2015, 26, 1850−1861

(30) Eichhorn, M. E., Strieth, S., and Dellian, M. (2004) Anti-vascular tumor therapy: recent advances, pitfalls and clinical perspectives. *Drug Resist. Updates 7*, 125−38.
(31) Willett, C. G., Boucher, Y., di Tomaso, E., Duda, D. G., Munn, L. L., Tong, R. T., Chung, D. C., Sahani, D. V., Kalva, S. P., Kozin, S. V., et al. (2004) Direct evidence that the VEGF-specific antibody bevacizumab has antivascular effects in human rectal cancer. *Nat. Med. 10*, 145−7.
(32) Fernando, N. H., and Hurwitz, H. I. (2003) Inhibition of vascular endothelial growth factor in the treatment of colorectal cancer. *Semin. Oncol. 30*, 39−50.
(33) Forsyth, P. A., Wong, H., Laing, T. D., Rewcastle, N. B., Morris, D. G., Muzik, H., Leco, K. J., Johnston, R. N., Brasher, P. M., Sutherland, G., and Edwards, D. R. (1999) Gelatinase-A (MMP-2), gelatinase-B (MMP-9) and membrane type matrix metalloproteinase-1 (MT1-MMP) are involved in different aspects of the pathophysiology of malignant gliomas. *Br. J. Cancer 79*, 1828−35.
(34) Roodink, I., and Leenders, W. P. (2010) Targeted therapies of cancer: Angiogenesis inhibition seems not enough. *Cancer Lett. 299*, 1−10.
(35) de Groot, J. F., Fuller, G., Kumar, A. J., Piao, Y., Eterovic, K., Ji, Y., and Conrad, C. A. (2010) Tumor invasion after treatment of glioblastoma with bevacizumab: radiographic and pathologic correlation in humans and mice. *Neuro Oncol. 12*, 233−42.
(36) Rubenstein, J. L., Kim, J., Ozawa, T., Zhang, M., Westphal, M., Deen, D. F., and Shuman, M. A. (2000) Anti-VEGF antibody treatment of glioblastoma prolongs survival but results in increased vascular cooption. *Neoplasia 2*, 306−14.
(37) Wang, Z., and Ho, P. C. (2010) A nanocapsular combinatorial sequential drug delivery system for antiangiogenesis and anticancer activities. *Biomaterials 31*, 7115−23.
(38) Zhang, B., Wang, H., Liao, Z., Wang, Y., Hu, Y., Yang, J., Shen, S., Chen, J., Mei, H., Shi, W., et al. (2014) EGFP-EGF1-conjugated nanoparticles for targeting both neovascular and glioma cells in therapy of brain glioma. *Biomaterials 35*, 4133−45.
(39) Rybak, J. N., Trachsel, E., Scheuermann, J., and Neri, D. (2007) Ligand-Based Vascular Targeting of Disease. *ChemMedChem 2*, 22−40.
(40) Ernsting, M. J., Murakami, M., Roy, A., and Li, S. D. (2013) Factors controlling the pharmacokinetics, biodistribution and intratumoral penetration of nanoparticles. *J. Controlled Release 172*, 782−94.
(41) Li, S. D., and Huang, L. (2008) Pharmacokinetics and biodistribution of nanoparticles. *Mol. Pharmaceutics 5*, 496−504.
(42) Discher, D. E., Ortiz, V., Srinivas, G., Klein, M. L., Kim, Y., Christian, D., Cai, S., Photos, P., and Ahmed, F. (2007) Emerging applications of polymersomes in delivery: from molecular dynamics to shrinkage of tumors. *Prog. Polym. Sci. 32*, 838−857.
(43) Hu, Q., Gao, X., Kang, T., Feng, X., Jiang, D., Tu, Y., Song, Q., Yao, L., Jiang, X., Chen, H., and Chen, J. (2013) CGKRK-modified nanoparticles for dual-targeting drug delivery to tumor cells and angiogenic blood vessels. *Biomaterials 34*, 9496−9508.
(44) Moghimi, S. M., and Hunter, A. C. (2001) Capture of stealth nanoparticles by the body's defences. *Crit. Rev. Ther. Drug Carrier Syst. 18*, 18−24.
(45) Kang, T., Gao, X., Hu, Q., Jiang, D., Feng, X., Zhang, X., Song, Q., Yao, L., Huang, M., Jiang, X., et al. (2014) iNGR-modified PEG-PLGA nanoparticles that recognize tumor vasculature and penetrate gliomas. *Biomaterials 35*, 4319−32.
(46) Hu, Q., Gao, X., Gu, G., Kang, T., Tu, Y., Liu, Z., Song, Q., Yao, L., Pang, Z., Jiang, X., et al. (2013) Glioma therapy using tumor homing and penetrating peptide functionalized PEG-PLA nanoparticles loaded with paclitaxel. *Biomaterials 34*, 5640−50.
(47) Gu, G., Xia, H., Hu, Q., Liu, Z., Jiang, M., Kang, T., Miao, D., Tu, Y., Pang, Z., Song, Q., et al. (2013) PEG-co-PCL nanoparticles modified with MMP-2/9 activatable low molecular weight protamine for enhanced targeted glioblastoma therapy. *Biomaterials 34*, 196−208.
(48) Pang, Z., Gao, H., Yu, Y., Guo, L., Chen, J., Pan, S., Ren, J., Wen, Z., and Jiang, X. (2011) Enhanced intracellular delivery and chemotherapy for glioma rats by transferrin-conjugated biodegradable polymersomes loaded with doxorubicin. *Bioconjugate Chem. 22*, 1171−80.

DOI: 10.1021/acs.bioconjchem.5b00379
Bioconjugate Chem. 2015, 26, 1850−1861